952

Intensity Distribution in Powder X-ray Diffraction from Nonstoichiometric Titanium Sulfide Containing Stacking Faults

By Mitsuko Onoda, Masanobu Saeki and Isao Kawada

National Institute for Researches in Inorganic Materials, Sakura-mura, Niihari-gun, Ibaraki, 305, Japan

Abstract

An expression for intensity distribution in powder X-ray diffraction from a sample containing stacking faults is derived. The analysis has been made for an experimental powder pattern of faulted $TiS_{1.56}$ which was prepared by reducing TiS_2 in an $H_2S–H_2$ atmosphere at 683 K. A model is assumed in which slides that cause the faults take place only between the S–Ti–S sandwiches. The experimental result is satisfactorily interpreted on the basis of the model.

Introduction

The layer units for the analysis of titanium sulfide with stacking faults were previously considered and the calculation procedure of the distribution of X-ray diffraction intensity along the reciprocal-lattice line has been described (Onoda & Kawada, 1980). At times, only the polycrystalline specimen is obtained, so it is important practically to analyze the powder X-ray pattern of faulted titanium sulfide. In this paper, the analysis of faulted titanium sulfide was attempted by comparing the experimental powder pattern with the calculated profile based on a model.

Expression for intensity distribution in powder X-ray diffraction

According to the powder-pattern power theorem (Warren, 1941, 1959), the total diffracted power is given by

$$P = \frac{R^2 M \lambda^3}{4} \int \frac{I(\xi,\eta,\zeta)}{\sin \theta} \, dV(RS)$$

$$= \frac{R^2 M \lambda^3}{4v_a} \int \int \int \frac{I(\xi,\eta,\zeta)}{\sin \theta} \, d\xi \, d\eta \, d\zeta, \quad (1)$$

where R is the distance from the sample to the receiving surface, M is the number of crystals, ξ, η and ζ are continuous coordinates along $\mathbf{a}^*$, $\mathbf{b}^*$ and $\mathbf{c}^*$, $dV(RS)$ is a volume element in reciprocal space, and v_a is the

volume of the unit cell. The intensity, $I(\xi,\eta,\zeta)$, of the diffuse scattering from a one-dimensionally faulted crystal is expressed by

$$I(\xi,\eta,\zeta) = N_3 L(\xi,\eta)D(\zeta), \quad (2)$$

where N_3 is the number of layers, $L(\xi,\eta)$ is the Laue function along $\mathbf{a}^*$ and $\mathbf{b}^*$, and $D(\zeta)$ is the intensity distribution along the reciprocal-lattice line, such as $10.\zeta$. We have

$$\xi = h + u, \quad \eta = k + v, \quad (3)$$

where h and k are integral indices, and u and v are small fractions of a reciprocal-lattice unit. Then

$$P = \frac{R^2 M \lambda^3}{4v_a} \int \int \int \frac{N_3 L(u,v)D(\zeta)}{\sin \theta} \, du \, dv \, d\zeta$$

$$= \frac{R^2 M \lambda^3}{4v_a} N_1 N_2 N_3 \int \frac{D(\zeta)}{\sin \theta} \, d\zeta. \quad (4)$$

For $\zeta \gg u$ and $\zeta \gg v$, that is for $d^* > d_0^*$ or $\sin \theta > \sin \theta_0$ where d^* is the distance of $\xi\eta\zeta$ from the origin of the reciprocal lattice and d_0^* is that of $hk0$, and 2θ and $2\theta_0$ are the diffraction angles corresponding to d^* and d_0^*,

$$\zeta^2 c^{*2} = d^{*2} - d_0^{*2} = \frac{4}{\lambda^2} (\sin^2 \theta - \sin^2 \theta_0), \quad (5)$$

and

$$d\zeta = \frac{d^*}{\zeta c^{*2}} d(d^*) = \frac{\sin \theta \cos \theta}{\lambda c^*(\sin^2 \theta - \sin^2 \theta_0)^{1/2}} d(2\theta). \quad (6)$$

Then

$$P = \frac{R^2 M \lambda^2 N_1 N_2 N_3}{4v_a c^*} \int \frac{D'(2\theta) \cos \theta}{(\sin^2 \theta - \sin^2 \theta_0)^{1/2}} d(2\theta). \quad (7)$$

Where $D(\zeta)$, which is numerically calculated in the manner described in the previous paper (Onoda & Kawada, 1980) as a function of ζ based on a model, is converted into $D'(2\theta)$ in such a way that the value of $D'(2\theta)$ is equal to that of $D(\zeta)$ under the condition that 2θ corresponds to ζ by the relation (5). P is expressed by using the diffracted power per unit angle $P_{2\theta}$ as

$$P = \int P_{2\theta} \, d(2\theta). \quad (8)$$

Accordingly,

$$P_{2\theta} = \frac{R^2 M \lambda^2 N_1 N_2 N_3}{4 v_a c^*} \frac{D'(2\theta) \cos \theta}{(\sin^2 \theta - \sin^2 \theta_0)^{1/2}}. \quad (9)$$

Since six $hk.\zeta$ reflexions and six $kh.\zeta$ reflexions contribute to the powder intensity of the same diffraction angle 2θ, the power per unit length of the Debye ring which is observed by using a powder diffractometer can be expressed as follows after introducing the polarization factor:

$$P'_{2\theta} = K \frac{1 + \cos^2 2\theta}{\sin \theta (\sin^2 \theta - \sin^2 \theta_0)^{1/2}} |D'_+(2\theta) + D'_-(2\theta)|, \quad (10)$$

where $D'_+(2\theta)$ and $D'_-(2\theta)$ are $D'(2\theta)$ due to $hk.\zeta$ and $kh.\zeta$ respectively. Equation (10) is substantially equal to the expression given by Warren (1941) and Brindley & Méring (1948).

For $d^* \simeq d_0^*$ or $\sin \theta \simeq \sin \theta_0$, the integration in (1) is more complex. After application of Warren's approximation, the following expression is obtained:

$$P'_{2\theta} = K \times 2 \left(\frac{S}{\sqrt{\pi \lambda}}\right)^{1/2} \frac{(1 + \cos^2 2\theta)}{(\sin \theta)^{3/2}} F(a)$$

$$\times |D'_+(2\theta) + D'_-(2\theta)|, \quad (11)$$

where S is the quantity which has the significance of a particle dimension, and a is $(2\sqrt{\pi}S/\lambda)(\sin \theta - \sin \theta_0)$. The function $F(a)$ is defined by

$$F(a) = \int_0^\infty \exp[-(x^2 - a)^2] \, dx, \quad (12)$$

and the value of $F(a)$ was given by Warren (1941).

When the temperature factors are treated as an overall isotropic temperature factor, then the intensity distribution profile $f(2\theta)$ is written as

$$f(2\theta) = \exp[-2B(\sin \theta/\lambda)^2] P'_{2\theta}, \quad (13)$$

where $P'_{2\theta}$ is expressed by (10) or (11).

If it is assumed that the superposition theorem holds, the experimental profile, $I_D(2\theta)$, is expressed by the convolution of the real profile, $f(2\theta)$, and the instrumental factor, $g(2\theta', 2\theta - 2\theta')$.

$$I_D(2\theta) = \int_{-\infty}^\infty f(2\theta')g(2\theta', 2\theta - 2\theta') \, d(2\theta'), \quad (14)$$

where $g(2\theta', 2\theta - 2\theta')$ is approximated by the sum of two asymmetric modified Lorentzian curves (Malmros & Thomas, 1977), which correspond to $K\alpha_1$ and $K\alpha_2$ peaks as follows:

$$g(2\theta', 2\theta - 2\theta') = \tfrac{2}{3}A(2\theta, 2\theta' - \Delta_1) ML(2\theta, 2\theta' - \Delta_1)$$

$$+ \tfrac{1}{3}A(2\theta, 2\theta' + \Delta_2)$$

$$\times ML(2\theta, 2\theta' + \Delta_2), \quad (15)$$

where

$$ML(2\theta, 2\theta') = \frac{4(\sqrt{2} - 1)^{1/2}}{H_k}$$

$$\times \left[1 + \frac{4(\sqrt{2} - 1)}{H_k^2} (2\theta - 2\theta')^2\right]^{-2}, \quad (16)$$

$$A(2\theta, 2\theta') = 1 - sP(2\theta - 2\theta')^2/\tan \theta', \quad (17)$$

$$H_k^2 = U \tan^2 \theta' + V \tan \theta' + W, \quad (18)$$

$$\Delta_1 = 2\theta'_{K\alpha} - 2\theta'_{K\alpha_1}, \quad \Delta_2 = 2\theta'_{K\alpha_2} - 2\theta'_{K\alpha}, \quad (19)$$

and s is the sign of $(2\theta - 2\theta')$. The parameters U, V and W, which determine the full width at half maximum H_k, and the asymmetry parameter P are determined by referring to the experimental profile obtained from a faultless Ti_2S_3 sample. $f(2\theta)$ and $g(2\theta', 2\theta - 2\theta')$ are substituted in (14), then the profile obtained is compared with the experimental powder pattern.

Interpretation of experimental powder pattern

Experimental

A sample of the TiS_2 phase was first synthesized from Ti metal powder (purity 99·0%) and S powder (99·9999%) in an evacuated quartz tube. The reaction was allowed to take place for a few days at 623 K and was subsequently carried out at 1173 K. The sample was then reduced at 683 K for 8 h in a stream of mixed H_2S and H_2 gas, whose ratio was regulated to be 1:400, and quenched. The composition of the sample was determined by weight-loss on oxidation to TiO_2 in air at 1073 K. The powder X-ray diffraction pattern was taken with Ni-filtered Cu $K\alpha$ radiation by a counter diffractometer. The measurement was carried out at a scanning speed of 1° (2θ) per 4 min.

The powder pattern of the sample having the analyzed composition of $TiS_{1.56}$ could be indexed on the basis of a CdI_2-type hexagonal lattice except for a few weak peaks. Selective broadening and weakening of

$Ti_{1.282} S_2 (TiS_{1.56})$
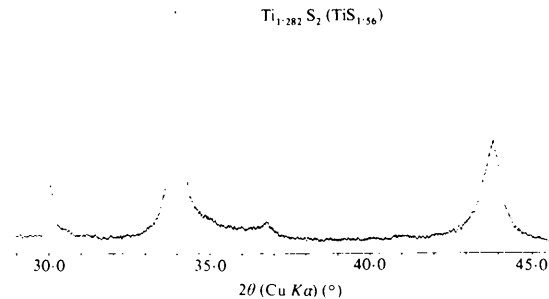
$2\theta (Cu K\alpha) (°)$

Fig. 1. Powder pattern of $TiS_{1.56}$ containing stacking faults.

the reflections was observed with $h - k \neq 3n$, so that the occurrence of stacking faults was suggested. The powder pattern ($30° < 2\theta < 45°$) obtained is shown in Fig. 1.

Structural models and calculated intensity distributions

The simplest model is that in which the hexagonal-close-packed S layer in the TiS_2-type structure is randomly substituted with the cubic-close-packed layer in the process of reduction. A S layer with a successive Ti layer was adopted as a layer unit. There are four kinds of fundamental units ($1A$, $2A$, $3A$ and $4A$), as shown in Fig. 3 in Onoda & Kawada (1980). They are described as Ab, Ab', Ac and Ac' respectively, with the notation that A, B and C represent S layers, a, b and c represent fully occupied Ti layers, and a', b' and c' represent partially occupied Ti layers. When the substitution probabilities are assumed to be equal for all S layers, $1A$, $2A$, $3A$ and $4A$ are followed respectively by $2C$, $1C$, $4B$ and $3B$ at probability α and by $4C$, $3C$, $2B$ and $1B$ at probability $(1 - \alpha)$. In this manner the P table was obtained, and $D(\zeta)$ was calculated numerically in Onoda & Kawada (1980). In the present study $D(\zeta)$ is converted into $D'(2\theta)$ by using the relation

$$\left(\frac{2 \sin \theta}{\lambda}\right)^2 = (h^2 + hk + k^2)a^{*2} + \zeta^2 c^{*2}. \quad (20)$$

By using a lattice constant ($a = 3\cdot43$ Å) and the thickness of the layer unit ($c = 2\cdot86$ Å), the values of a^* and c^* are calculated at $2/(\sqrt{3} \times 3\cdot43)$ Å^{-1} and $1/2\cdot86$ Å^{-1} respectively. The intensity distribution is obtained from (10)–(19), and the intensity curves obtained on the assumptions $S = 10\,000$ Å and $B = 1\cdot0$ are illustrated in Fig. 2. The curve for $\alpha = 0\cdot1$ is in close agreement with the experimental result. However, a weak peak observed at $2\theta = 36\cdot8°$ in Fig. 1, which corresponds to $\zeta = 0\cdot6667$, could not be explained.

Furthermore, a case was examined in which the fault probability in the S layer over the partially occupied Ti layer was different from that over the fully occupied Ti layer. However, the profile shown in Fig. 1 is still not adequately explained. Therefore, an extended model is needed.

A set of two subsequent S layers and a fully occupied Ti layer inserted between them is named a sandwich. A crystal of TiS_2-type nonstoichiometric titanium sulfide contains partially occupied Ti layers, which are named Ti' layers, and only positive sandwiches or negative sandwiches, where the terms positive and negative are used to distinguish between changes of the successive S sites composing the sandwiches for increasing z, $A \to B \to C \to A$ and $A \to C \to B \to A$ respectively. A model is considered in which the cubic-close-packed S layer is introduced into the TiS_2-type structure in the process of reduction in the following manner. A slide causes the faults, and it is assumed that a slide takes place only between the sandwiches. When faults are introduced into a crystal containing only the positive sandwiches and the Ti' layers, the faulted crystal also only contains positive sandwiches and Ti' layers, as shown in Fig. 3.

The layer units whose thicknesses are all equal to twice the layer thickness of the simple model are adopted. They are composed of two S layers, one fully occupied Ti layer, half of a partially occupied Ti layer, and half of another partially occupied Ti layer, as shown in Onoda & Kawada (1980).

These layer units, $1A$, $2A$, ... and $8A$, are shown in a different manner in Fig. 4. The crystal containing only the positive sandwiches can be treated on the basis of four kinds of layer units, $2A$, $3A$, $5A$, and $8A$ only, for the present model, while the crystal containing only the
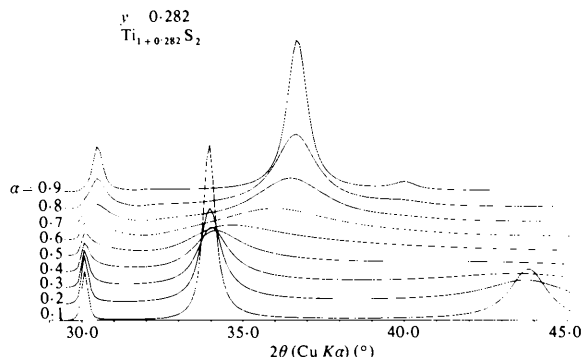

Fig. 2. Calculated intensity curves for the model in which a hexagonal-packed S layer in the TiS_2-type structure is substituted for a cubic-packed layer with probability α. The value used for y in $Ti_{1+y}S_2$ is $0\cdot282$.
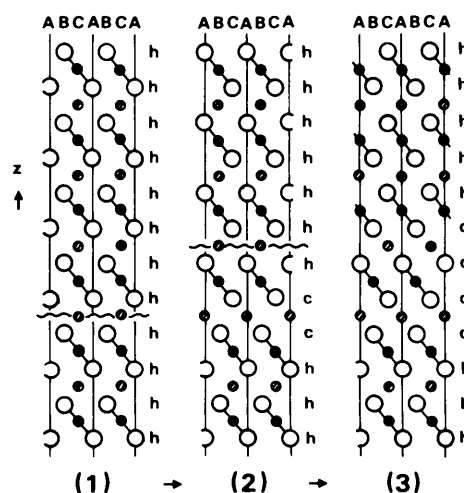

Fig. 3. The mode of formation of the stacking faults caused by the slides between the sandwiches. A line of linkages of two O and one ● indicates a S–Ti–S sandwich. O S site; ● fully occupied Ti site; ⊘ partially occupied Ti site.

the negative sandwiches can be treated on the basis of the layer units $1A$, $4A$, $6A$, and $7A$. The layer units are rearranged, and the **P** table shown in Table 1 is obtained for the positive crystal. The layer form factors are expressed as

$$V_{1'} = V_8 = L^{1/2}(\xi,\eta)\{(yf_{Ti}/2)\,[1 + \exp(-i2\pi\zeta)]$$
$$+ f_S\,\varepsilon^*\exp(-i\pi\zeta/2) + f_{Ti}\exp(-i\pi\zeta)$$
$$+ f_S\,\varepsilon\exp(-i3\pi\zeta/2)\},$$

$$V_{2'} = V_5 = L^{1/2}(\xi,\eta)\{(yf_{Ti}/2)\,[\varepsilon + \exp(-i2\pi\zeta)]$$
$$+ f_S\,\varepsilon^*\exp(-i\pi\zeta/2) + f_{Ti}\exp(-i\pi\zeta)$$
$$+ f_S\,\varepsilon\exp(-i3\pi\zeta/2)\}, \qquad (21)$$

$$V_{3'} = V_3 = L^{1/2}(\xi,\eta)\{(yf_{Ti}/2)\,[\varepsilon + \exp(-i2\pi\zeta)]$$
$$+ f_S\exp(-i\pi\zeta/2) + f_{Ti}\,\varepsilon\exp(-i\pi\zeta)$$
$$+ f_S\,\varepsilon^*\exp(-i3\pi\zeta/2)\},$$

$$V_{4'} = V_2 = L^{1/2}(\xi,\eta)\{(yf_{Ti}/2)\,[\varepsilon^* + \exp(-i2\pi\zeta)]$$
$$+ f_S\exp(-i\pi\zeta/2) + f_{Ti}\,\varepsilon\exp(-i\pi\zeta)$$
$$+ f_S\,\varepsilon^*\exp(-i3\pi\zeta/2)\},$$

where $L(\xi,\eta)$ is the Laue function involving $\mathbf{a}^*$ and $\mathbf{b}^*$, f_S and f_{Ti} are the atomic scattering factors for the S and Ti ions respectively, y is the occupancy factor of the partially occupied Ti layer and the composition is represented by $Ti_{1+y}S_2$. ζ is the coordinate along $\mathbf{c}^*$, where c^* is the reciprocal of the thickness of the layer unit ($c = 5.72$ Å). The existence probabilities are obtained as

$$w_{1'} = (1 - \alpha_2)(1 - \alpha_4)/[(1 - \alpha_2)\,(1 - \alpha_4)$$
$$+ 2\alpha_1(1 - \alpha_4) + \alpha_1\,\alpha_3],$$

$$w_{2'} = w_{3'} = \alpha_1(1 - \alpha_4)/[(1 - \alpha_2)\,(1 - \alpha_4)$$
$$+ 2\alpha_1(1 - \alpha_4) + \alpha_1\,\alpha_3], \qquad (22)$$

$$w_{4'} = \alpha_1\,\alpha_3/[(1 - \alpha_2)\,(1 - \alpha_4) + 2\alpha_1(1 - \alpha_4)$$
$$+ \alpha_1\,\alpha_3],$$

and intensity distributions for $10.\zeta$ and $01.\zeta$ are calculated according to the procedures described in Onoda & Kawada (1980). The intensity distribution for a crystal containing only negative sandwiches is obtained in a similar manner as given above. The total intensity distribution is obtained from the sum of both distribution curves, because a powder sample contains crystals made up of positive sandwiches and crystals made up of negative sandwiches in equal amounts. The sum of $D(\zeta)$ is converted into $D'(2\theta)$ by using the value $c^* = 1/5.72$ Å^{-1}. The calculated intensity curves for powder X-ray diffraction are obtained according to the same procedure as that described for the simple model. When $\alpha_1 = \alpha_2 = \alpha_3 = \alpha_4$, the change of the calculated curve for increasing α_1 closely resembles that shown in Fig. 2, and the experimental result is not adequately explained. With the assumption that $\alpha_1 = \alpha_2 \neq \alpha_3 = \alpha_4$,

the intensity distributions have been calculated by using the various values of α_1 and α_3, and a curve for $\alpha_1 = 0.08$ and $\alpha_3 = 0.65$ is in close agreement with the experimental result, as shown in Fig. 5(a). Next, the intensity distributions have been calculated by specifying the respective values of α_1, α_2, α_3 and α_4. The curve calculated for $\alpha_1 = 0.08$, $\alpha_2 = 0.40$, $\alpha_3 = 0.10$ and $\alpha_4 = 0.82$ is demonstrated in Fig. 5(b), and it gives a satisfactory explanation of the experimental result including the weak peaks.

Discussion

The layer-unit expressions such as $a^-(h + h)a^-$, $c^+(c + h)a^-$, etc., described in Onoda & Kawada (1980), are simplified as (hh), (ch), etc., by extracting the S packing character. The probability table arranged by the use of the simplified expressions is shown in Table 2. This means that (hh) is followed by (hh) at the probability of $(1 - \alpha_1)$ and by (hc) at the probability of α_1 and so forth. In the case of Fig. 5(a), both (hh) and (ch) are
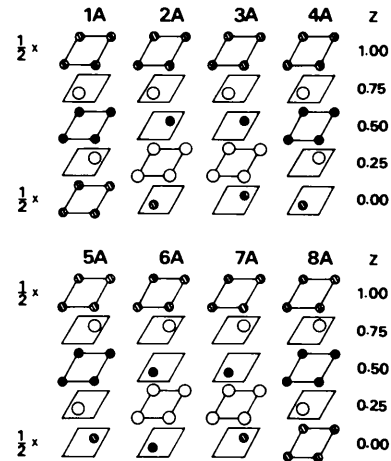

Fig. 4. Layer units containing two S layers. ◯ S site; ● fully occupied Ti site; ◉ partially occupied Ti site.
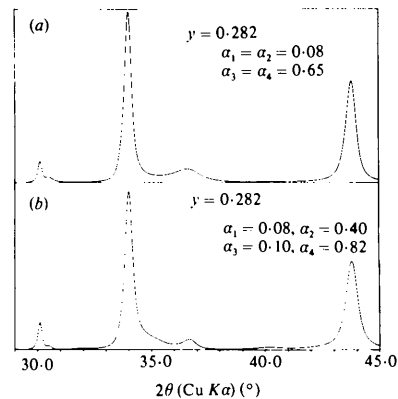

Fig. 5. Intensity curves calculated for the model of Table 1. A value of 0.282 is used for y in $Ti_{1+y}S_2$.

Table 1. **P** *table based on the extended model by using only the positive layer units illustrated in Fig. 4*

	1'A	2'A	3'A	4'A	1'B	2'B	3'B	4'B	1'C	2'C	3'C	4'C
a⁻(h+h)a⁻ 8A = 1'A	$1-\alpha_1$									α_1		
c⁺(c+h)a⁻ 5A = 2'A	$1-\alpha_2$									α_2		
c⁻(h+c)a⁺ 3A = 3'A							$1-\alpha_3$					α_3
b⁺(c+c)a⁺ 2A = 4'A							$1-\alpha_4$					α_4
b⁻(h+h)b⁻ 8B = 1'B					$1-\alpha_1$							α_1
a⁺(c+h)b⁻ 5B = 2'B					$1-\alpha_2$							α_2
a⁻(h+c)b⁺ 3B = 3'B							$1-\alpha_3$				α_3	
c⁺(c+c)b⁺ 2B = 4'B							$1-\alpha_4$				α_4	
c⁻(h+h)c⁻ 8C = 1'C		α_1							$1-\alpha_1$			
b⁺(c+h)c⁻ 5C = 2'C		α_2							$1-\alpha_2$			
b⁻(h+c)c⁺ 3C = 3'C	$1-\alpha_3$										α_3	
a⁺(c+c)c⁺ 2C = 4'C	$1-\alpha_4$										α_4	

Table 2. *Probability table set from Table 1 by using simplified expressions of stacking layers*

	(hh)	(ch)	(hc)	(cc)
(hh)	$1-\alpha_1$		α_1	
(ch)	$1-\alpha_2$		α_2	
(hc)		$1-\alpha_3$		α_3
(cc)		$1-\alpha_4$		α_4

followed by (hh) at the equal probability $(1 - \alpha_1)$ and (hc) at α_1 and so on. This case corresponds to the existence of a slide at a Ti' layer having no influence on the probability of slide at the second-nearest Ti' layer. This model gives close agreement, but it does not explain adequately the fine features of the experimental pattern, such as the broadness of the peak at $2\theta = 36 \cdot 8°$ and the slight elevation near $2\theta = 35 \cdot 0°$. In the case of Fig. 5(b), the existence of a slide at a Ti' layer influences the probability of a slide at the second-nearest Ti' layer. This case gives a satisfactory explanation. In order to obtain the microscopic model of S stacking sequences from the values of the parameters α_1 to α_4, a simulation has been attempted by using the random-number table. Part of the model obtained for the case of Fig. 5(b) is as follows: ... (hh) (hh) (hh) (hh) (hh) (hc) (cc) (cc) (cc) (cc) (cc) (cc) (cc) (cc) (ch) (hh) (hh) (hh) (hh) (hh) (hh) (hh) (hh) (hh) (hh) (hh) (hh) (hh) (hh) (hh) (hh) (hh) (hh) (hh) (hh) (hh) (hh) (hh) (hc) (ch) (hh) (hh) (hh) (hh) (hh) (hh) (hh) (hh) (hh) (hh) (hh) (hh) (hh) (hh) (hh) (hh) (hh) (hh) (hh) (hh) (hh) (hh) (hh) (hh) (hh) (hh) (hh) (hh) (hc) (ch) (hc) (ch) (hh) (hc) (ch) (hc) (ch) (hh) (hh) (hh) (hh) (hh) (hh) (hh) (hh) (hh) (hh) ..... Why different values of the parameters give apparently similar curves in the cases of Fig. 5(a) and (b) can be explained as follows. The values of $(1 - \alpha_1)$ and α_4 seem to determine the broadness of the peaks, while the values of α_2 and α_3 seem to determine the height ratios of the peaks and the extents of the trails. In the case of Fig. 5(a), the fitting was judged mainly by the broadness of the peak at $2\theta = 34 \cdot 0°$, which is related to α_1, and the height ratio of the peak at $2\theta = 34 \cdot 0°$ to that at $2\theta = 36 \cdot 8°$, which is related to α_2 and α_3. Then the assumption $\alpha_1 = \alpha_2 \neq \alpha_3 = \alpha_4$ may impose an inaccurate value on α_4 $(= \alpha_3)$, since incorrectly estimated α_2 must be compensated by shifts of α_3 and α_4.

Recently a new type of Ti_2S_3 has been found which is composed of cubic-close-packed S layers as well as the fully and partially occupied Ti layers, and is referred to as $6R$ type according to the Ramsdell notation (Onoda & Saeki, 1980). One may suspect that the weak peak at

$2\theta = 36 \cdot 8°$ arises from the existence of crystals of $6R$ type with stacking faults, since the strongest peak of $6R$ type is at $2\theta = 36 \cdot 8°$ and crystals of $6R$ type can be formed by slides between the S–Ti–S sandwiches from crystals of $2H$ type. However, it has been found that the lattice constants of the faulted crystals prepared under similar conditions to those used in the present study change gradually with the nonstoichiometric change of chemical composition (Saeki, Onoda, Kawada & Nakahira, 1980). In the binary systems such as the Ti–S system the mixture of two phases gives the two sets of lattice constants, which are related respectively to the two end compounds, and each set is not dependent on the total composition of the mixture, but on the individual composition of the end compounds. This being the case, the specimen is unlikely to be a mixture of faulted $2H$ crystals and faulted $6R$ crystals.

In the case of the extended model, the occurrence of stacking faults does not need slides within the sandwiches but does need slides between the sandwiches. In all probability the slide between the sandwiches occurs more easily than that within the sandwiches, because a slide of one S layer over the adjacent S layer needs a synchronous shear of the Ti layer inserted between the two S layers as shown in Fig. 6 and the shear of the partially occupied Ti layer is

Fig. 6. Atom movement during synchronous shear. The upper and lower figures are side and top views respectively. The solid arrows indicate the displacements of the S atoms and the broken arrows indicate those of the Ti atoms. O, ⌀ S atoms; ● Ti atom.

easier than that of the fully occupied Ti layer. It is probable that the stacking faults which occur at a low temperature such as 683 K are due only to the slide between the sandwiches, and the experimental data shown in Fig. 1 should be interpreted appropriately on the basis of the extended model.

Experimental patterns which suggest the occurrence of stacking faults are often observed for the various temperatures and compositions in the Ti–S system. The method of analysis of the structure with stacking faults described above may be effectively used for considering the phase-relation problem in this system.

References

BRINDLEY, G. W. & MÉRING, J. (1948). *Nature (London)*, **161**, 774–775.
MALMROS, G. & THOMAS, J. O. (1977). *J. Appl. Cryst.* **10**, 7–11.
ONODA, M. & KAWADA, I. (1980). *Acta Cryst.* A36, 134–139.
ONODA, M. & SAEKI, M. (1980). *Chem. Lett.* pp. 665–666.
SAEKI, M., ONODA, M., KAWADA, I. & NAKAHIRA, M. (1980). *J. Less-Common Met.* In the press.
WARREN, B. E. (1941). *Phys. Rev.* **59**, 693–698.
WARREN, B. E. (1959). *Prog. Met. Phys.* **8**, 147–202.

Dynamic Deformation and the Debye–Waller Factors for Silicon-Like Crystals

BY JOHN S. REID AND JOHN D. PIRIE

Department of Natural Philosophy, The University, Aberdeen AB9 2UE, Scotland

Abstract

Calculations are presented of the Debye–Waller factors for silicon, diamond and germanium in the temperature range 1 to 1000 K and for grey tin in the range 1 to 280 K. Values were obtained from the shell model, the adiabatic bond-charge model and the valence force potential model for all four materials. Further values are listed from the fitted Born–von Kármán model for silicon and germanium and from two additional parametrizations of the valence force potential model for silicon. The effect of dynamic deformation on the Debye–Waller factor of silicon and, to a slightly lesser extent, the other three elements, is investigated. The Debye–Waller factor for the shells only in the the shell models is calculated. The effect introduced by dynamic deformation whereby the Debye–Waller B value varies with scattering vector $\mathbf{K}$ is evaluated. Finally, the anisotropic Debye–Waller factor components for the bond charges are calculated for all four elements. It is found that the bond charges in the bond-charge model and the shells in the shell model vibrate substantially less than the main atomic cores. It is concluded that if the models are at all realistic then the effects of dynamic deformation on the Debye–Waller factors of these elements should be seriously considered.

Introduction

Interest in the scattering caused by dynamic deformation of electron distributions has arisen from essentially two different sources. On the one hand detailed investigation into thermal diffuse scattering processes has suggested that some contribution to the X-ray scattering is made by the deformation of the electron distribution during thermal vibration, as, for example, has been discussed by Buyers, Pirie & Smith (1968). On the other hand, very accurate crystallographic structural determinations are reaching the stage with favourable materials that different thermal motions of different parts of the electron distribution associated with one particular atom may be experimentally distinguished. An example of these possibilities has been discussed by Price, Maslen & Mair (1978) in the analysis of data for silicon.

In succeeding sections the aim is to bring the insight generated by thermal diffuse scattering studies to bear on the effect which is of most interest to the structural crystallographer, namely the Debye–Waller factor. Although particular emphasis is placed on providing numerical information for silicon, partly for comparison and partly for their intrinsic interest, additional calculations are presented for diamond, germanium and α-tin.

The dynamical deformation formalism is, essentially, a general parametric description of the influence of dynamically distorting electron distributions on the X-ray scattering. The formalism enables distorting atoms to be treated in a similar way to rigid atoms provided certain terms in the cross section are redefined so that, in effect, additional terms are added to the scattering cross sections. As a consequence, any cross